ACCURATE SHADOW REGION IMAGING ALGORITHM BASED ON DOUBLY SCATTERED RANGE POINTS MIGRATION FOR UWB RADARS

Shouhei Kidera and Tetsuo Kirimoto

Graduate School of Informatics and Engineering, University of Electro-Communications, Tokyo, Japan
Email: kidera@ee.uec.ac.jp

ABSTRACT

Ultra wideband (UWB) radar shows promise for near field measurement with its high range resolution, which is suitable for imaging sensors of rescue robots. Recently, radar algorithms employing multiple scattered components have been developed to enhance imaging range compared to that synthesized by a single scattered component. While, as such, we have already proposed a fast algorithm using ranges derivatives for double scattered signals, this cannot produce an accurate image for more complex-shaped objects or in noisy environments, because interference signals or random errors can produce non-negligible image degradation caused by its derivative operation. As a solution to this difficulty, this paper introduces a novel algorithm without using range derivatives but employing a global characteristic of double scattered range points. Some numerical simulation examples verify that this method can create more accurate images even for more interfered and noisy situations.

Index Terms— UWB radar, Doubly scattered wave, Shadow region imaging, Range points migration

1. INTRODUCTION

UWB pulse radar with high range resolution creates various applications for near field measurement techniques. A robotic sensor is one of the most promising applications, which is able to identify a human body even with optically blurry visibility such as dark smog in disaster areas or high-density gas in resource exploration situations. While various kinds of radar algorithms have been developed as the synthetic aperture radar (SAR) based schemes [1], the time reversal approach [2], or solutions for domain integral equations [3], they are not suitable for the above applications because, generally, it is difficult to achieve both low computation cost and high spatial resolution. As a high-speed and accurate imaging method applicable to complex-shaped or multiple targets, the Range Points Migration (RPM) algorithm has been established [4]. This algorithm directly estimates an accurate direction of arrival (DOA) derived from the global distribution of observed range points, avoiding the difficulty of connecting them. However, the RPM or other methods have the essential problem that the aperture size strictly constrains the reproducible range of the target boundary. In many cases, the greater part of a target shape, such as its side, falls into a shadow region that is never reconstructed since only single scattered components are used for imaging. To resolve this difficulty and enhance the visible area, image expansion algorithms based on double scattered signals have been developed [5, 6]. In particular, the method [6] successfully expands an imaging region with low computation, combining the RPM algorithm and original relationship established between the range derivatives and each DOA of the double scattering centers. However, in the case of complex shapes or noisy situations, it suffers from image degradation caused by situations subject to severe interference due to single scattered components or random noises, which can bring out the inaccuracy particular for the range derivative.

As an essential solution for this problem, this paper newly introduces a shadow region imaging algorithm that is based on an advanced RPM principle applied to the double scattered signals. A notable advantage of this method is that the shadow region is reproduced by employing not local, but global distribution of the observed range points. The results of numerical simulations show that the proposed method significantly enhances the reproducible range of target shapes including complex-shaped targets, and holds accuracy in noisy situations, which cannot be accomplished with the conventional algorithm.

2. SYSTEM MODEL

Fig. 1 shows the system model. It assumes a mono-static radar, with an omni-directional antenna scanned along the x-axis, and that the target has an arbitrary shape with a clear boundary. The propagation speed of the radio wave c is assumed to be a known constant. A mono-cycle pulse is used as the transmitting current. The real space in which the target and antenna are located, is expressed by the parameters (x, z). The parameters are normalized by λ which is the central wavelength of the pulse. $z > 0$ is assumed for simplicity. $s'(X, Z)$ is defined as the received electric field at the antenna location $(x, z) = (X, 0)$, where $Z = ct/(2\lambda)$ is a function of time t. $s(X, Z)$ is defined as the output of the Wiener fil-

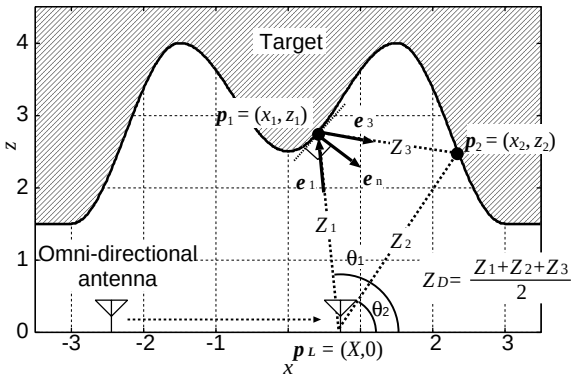

Fig. 1. System model and relationship among $\boldsymbol{p}_1$, $\boldsymbol{p}_2$ and $\boldsymbol{p}_L$.

ter with the transmitted waveform, which is detailed in [4]. The range points being candidates for single and double scattered echoes are defined as (X, Z_S) and (X, Z_D), which are extracted from the local maxima and minima of $s(X, Z)$, respectively.

3. CONVENTIONAL METHOD

We have already proposed a high-speed shadow region imaging algorithm, which employs target points initially created by the RPM method that uses single scattered components and the range derivatives of the double scattered signals [6]. Here, two target points originating from doubly scattering are defined as $\boldsymbol{p}_1 \equiv (x_1, z_1)$ and $\boldsymbol{p}_2 \equiv (x_2, z_2)$, respectively. $\boldsymbol{p}_L \equiv (X, 0)$ denotes an antenna location. This method uses the following relationship,

$$\partial Z_D/\partial X \quad = \quad -\left(\cos\theta_1 + \cos\theta_2\right)/2, \tag{1}$$

where $\theta_1 = \cos^{-1}\left((x_1 - X)/Z_1\right)$, $\theta_2 = \cos^{-1}\left((x_2 - X)/Z_2\right)$, $Z_1 = \|\boldsymbol{p}_1 - \boldsymbol{p}_L\|$ and $Z_2 = \|\boldsymbol{p}_2 - \boldsymbol{p}_L\|$ hold. Then, once $\boldsymbol{p}_1$ is determined, θ_2 is directly calculated in Eq. (1) with $\partial Z_D/\partial X$. Besides, if the normal vector $\boldsymbol{e}_{\rm n}$ on $\boldsymbol{p}_1$ is given, the law of reflection derives $Z_2 = Z_D - Z_1\frac{(Z_D - Z_1)(\boldsymbol{e}_1\cdot\boldsymbol{e}_{\rm n})^2}{Z_D - Z_1(\boldsymbol{e}_1\cdot\boldsymbol{e}_{\rm n})^2}$, where $\boldsymbol{e}_1 = (\boldsymbol{p}_1 - \boldsymbol{p}_L)/Z_1$ holds. Namely, $\boldsymbol{p}_2$ can be calculated from $\boldsymbol{p}_1$ and $\boldsymbol{e}_{\rm n}$ with $\partial Z_D/\partial X$. Furthermore, $\boldsymbol{p}_2$ satisfies $\boldsymbol{p}_2 = \boldsymbol{p}_1 + Z_3\boldsymbol{e}_3$, where $Z_3 \equiv \|\boldsymbol{p}_2 - \boldsymbol{p}_1\| = 2Z_D - Z_1 - Z_2$ and $\boldsymbol{e}_3 = \boldsymbol{e}_1 - 2(\boldsymbol{e}_{\rm n}\cdot\boldsymbol{e}_1)\boldsymbol{e}_{\rm n}$. Fig. 1 shows the relationship among the target points $\boldsymbol{p}_1$, $\boldsymbol{p}_2$ and the antenna location $\boldsymbol{p}_L$.

As the first scattering location $\boldsymbol{p}_1$ with its normal vector $\boldsymbol{e}_{\rm n}$, this method employs the initial target points using RPM defined as $\boldsymbol{p}^{\rm rpm}$ and its normal vector as $\boldsymbol{e}_{\rm n}^{\rm rpm}$, which is given by the direction of the line of sight from the antenna location [4]. Here, $\boldsymbol{Q}_i \equiv (X_i, Z_{D,i})$, $(i = 1, \cdots, N_{\rm Q})$ and $\boldsymbol{P}_j \equiv (\boldsymbol{p}_j^{\rm rpm}, \boldsymbol{e}_{{\rm n},j}^{\rm rpm})$, $(j = 1, \cdots, N_{\rm R})$ are defined, where $N_{\rm Q}$ and $N_{\rm R}$ denote the numbers of (X, Z_D) and the target points obtained by RPM. This algorithm determines an optimal $\boldsymbol{P}$ for $\boldsymbol{Q}_i$ using numerically calculated $\partial Z_{D,i}/\partial X_i$ as,

$$\tilde{\boldsymbol{P}}(\boldsymbol{Q}_i) \equiv \underset{\boldsymbol{P}_j\in\mathcal{P}_{\rm rpm}}{\arg\min} \left\|\boldsymbol{p}_2^A(\boldsymbol{Q}_i;\boldsymbol{P}_j) - \boldsymbol{p}_2^B(\boldsymbol{Q}_i, \partial Z_{D,i}/\partial X_i;\boldsymbol{P}_j)\right\|, \tag{2}$$

where $\mathcal{P}_{\rm rpm}$ is a set of $\boldsymbol{P}_j$, and

$$\boldsymbol{p}_2^A(\boldsymbol{Q}_i;\boldsymbol{P}_j) \equiv \boldsymbol{p}_j^{\rm rpm} + Z_3(\boldsymbol{Q}_i;\boldsymbol{P}_j)\boldsymbol{e}_3(\boldsymbol{Q}_i;\boldsymbol{P}_j), \tag{3}$$

$$\boldsymbol{p}_2^B(\boldsymbol{Q}_i, \partial Z_{D,i}/\partial X_i;\boldsymbol{P}_j) \equiv \boldsymbol{p}_{L,i} + Z_2(\boldsymbol{Q}_i;\boldsymbol{P}_j) \times \left(\cos\theta_2(\boldsymbol{Q}_i, \partial Z_{D,i}/\partial X_i;\boldsymbol{P}_j), \sin\theta_2(\boldsymbol{Q}_i, \partial Z_{D,i}/\partial X_i;\boldsymbol{P}_j)\right). \tag{4}$$

Then, the optimum second scattering point is determined as $\tilde{\boldsymbol{p}_2}(\boldsymbol{Q}_i) \equiv \dfrac{\boldsymbol{p}_2^A(\boldsymbol{Q}_i;\tilde{\boldsymbol{P}}(\boldsymbol{Q}_i)) + \boldsymbol{p}_2^B(\boldsymbol{Q}_i, \partial Z_{D,i}/\partial X;\tilde{\boldsymbol{P}}(\boldsymbol{Q}_i))}{2}$. Although this method accomplishes fast imaging without any integration process, it needs to employ the derivative operation of the range curves which could enhance small range fluctuations, that is, it suffers severely from degraded accuracy in the case of a complex-shaped target or in noisy situations.

4. PROPOSED METHOD

As a promising solution to the previous difficulty, this paper proposes a novel shadow region imaging algorithm that is not based on range derivatives, but exploits the global distribution of (X, Z_D). This method employs only the group of $\boldsymbol{p}_2^A(\boldsymbol{Q}_i;\boldsymbol{P}_j)$, which is defined in Eq. (3) with no derivative operation. Our method is based on the following two principles. The first is that, if $\boldsymbol{P}_j$ takes the actual $\boldsymbol{P}$, the closest point between $\boldsymbol{p}_2^A(\boldsymbol{Q}_i;\boldsymbol{P}_j)$ and $\boldsymbol{p}_2^A(\boldsymbol{Q}_k;\boldsymbol{P}_l)$ in changing $\boldsymbol{P}_l$ should converge around the actual secondary scattering point when $\boldsymbol{Q}_k \to \boldsymbol{Q}_i$. The second is that $\boldsymbol{p}_2^A(\boldsymbol{Q}_k;\boldsymbol{P}_l)$ should be located around the ellipse, whose focal points are $\boldsymbol{p}_{L,i}$ and $\boldsymbol{p}_j^{\rm rpm}$ and the major diameter is $2Z_{D,i} - \|\boldsymbol{p}_{L,i} - \boldsymbol{p}_j^{\rm rpm}\|$, according to the law of reflection. Fig. 2 illustrates the relationship among $\boldsymbol{p}_2^A(\boldsymbol{Q}_i;\boldsymbol{P}_j)$, $\boldsymbol{p}_2^A(\boldsymbol{Q}_k;\boldsymbol{P}_l)$ and the above ellipse. Based on these principles, this method calculates the optimum first scattering parameter $\hat{\boldsymbol{P}}(\boldsymbol{Q}_i)$ as

$$\hat{\boldsymbol{P}}(\boldsymbol{Q}_i) \equiv \underset{\boldsymbol{P}_j\in\mathcal{P}_{\rm rpm}}{\arg\max} \sum_{k=1}^{N_{\rm Q}} s(\boldsymbol{Q}_k)\exp\left(-\frac{|X_i - X_k|^2}{2\sigma_X^2}\right) \times \exp\left(-\frac{\left|\left(\boldsymbol{p}_2^A(\boldsymbol{Q}_i;\boldsymbol{P}_j) - \boldsymbol{p}_2^A(\boldsymbol{Q}_k;\boldsymbol{P}')\right)\cdot\boldsymbol{e}_{{\rm n},2}(\boldsymbol{Q}_i;\boldsymbol{P}_j)\right|^2}{2\sigma_{\rm p}^2}\right), \tag{5}$$

where $\boldsymbol{P}' \equiv \underset{\boldsymbol{P}_l\in\mathcal{P}_{\rm rpm}}{\arg\min} \left\|\boldsymbol{p}_2^A(\boldsymbol{Q}_i;\boldsymbol{P}_j) - \boldsymbol{p}_2^A(\boldsymbol{Q}_k;\boldsymbol{P}_l)\right\|$, and $\boldsymbol{e}_{{\rm n},2}(\boldsymbol{Q}_i;\boldsymbol{P}_j)$ denote the normal vector on $\boldsymbol{p}_2^A(\boldsymbol{Q}_i;\boldsymbol{P}_j)$, which is determined by $\boldsymbol{p}_j^{\rm rpm}$ and $\boldsymbol{p}_{L,i}$ with the law of reflection. σ_X and $\sigma_{\rm p}$ are empirically determined constants.

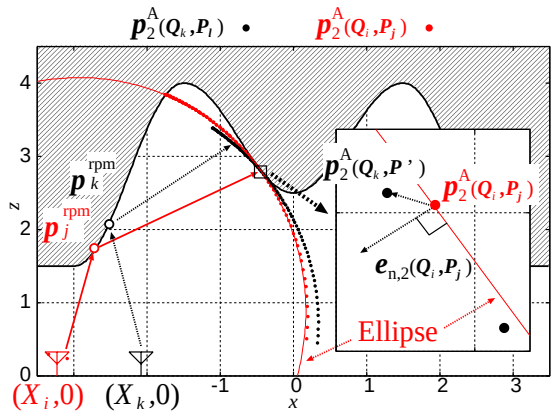

Fig. 2. Relationship among $p_2^A(Q_i;P_j)$, $p_2^A(Q_k;P_l)$ and the ellipse.

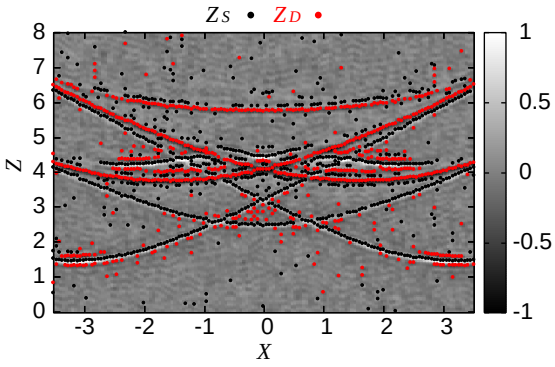

Fig. 3. Output of Wiener filter and extracted range points (X, Z_S) and (X, Z_D) in the case of Fig. 1 at S/N $= 20$ dB.

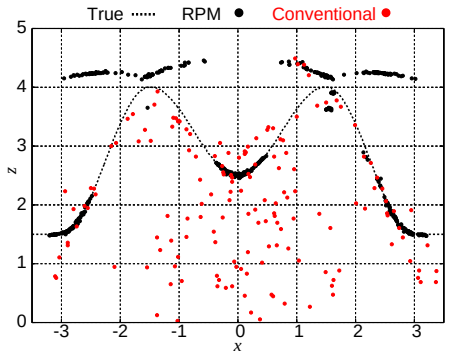

Fig. 4. Estimated image with RPM and the conventional method at S/N $= 20$ dB.

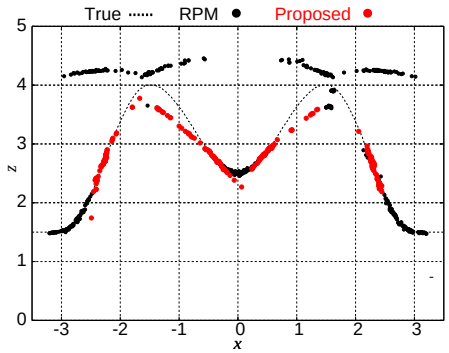

Fig. 5. Estimated image with RPM and the proposed method at S/N $= 20$ dB.

The right term of Eq. (5) measures the convergence degree in terms of antenna locations, considering the distance to the ellipse tangent to the target boundary. Finally, the second scattering point $\hat{p}_2$ for Q_i is calculated as $\hat{p}_2(Q_i) \equiv p_2^A(Q_i, \hat{P}(Q_i))$. This method does not require the derivative operation for the shadow region imaging, and is less sensitive to the small range fluctuations owing to random components or interference echoes from other scattering locations.

5. PERFORMANCE EVALUATION IN NUMERICAL SIMULATION

This section presents numerical examples performed using each method in noisy situations, whereby white Gaussian noise is added to each received signal as $s'(X, Z)$. Fig. 3 shows the output of the Wiener filter and each of the extracted range points (X, Z_S) and (X, Z_D), where the target boundary is assumed to be the same as in Fig. 1, and the mean S/N is around 20 dB. The S/N is defined as the ratio of peak signal power to the averaged noise power after applying the matched filter with the transmitted waveform. The received signals are calculated at 141 locations for $-3.5\lambda \geq x \geq 3.5\lambda$ using FDTD (Finite Difference Time Domain) method. Fig. 4 presents the estimated target points using the RPM [4] and the conventional method [6], and indicates that the estimated secondary scattering points are far from the actual boundary, and it hardly offers a meaningful image for shadow region. The reason is that the calculation of $\partial Z_D/\partial X$ essentially suffers from an inaccuracy owing to the intensive interfered or random components as in Fig. 3. On the contrary, Fig. 5 shows the target points obtained by the proposed method, for which the same data as in Fig. 3 is used. $\sigma_{\rm p} = 0.05\lambda, \sigma_X = 2.0\lambda$ are set. As shown in this figure, our method creates only accurate target points, because it employs a global distribution of the range points (X, Z_D), which can suppress image distortions caused by range fluctuations owing to interferences or random noises. Obviously, both images with the RPM and the proposed method are useful for object recognition. Note that, there are some false images by RPM over the actual boundary, which are caused by more than triple scattering components.

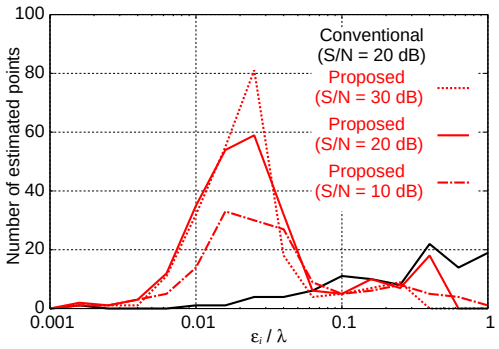

Fig. 6. Number of target points for each ϵ_i in some S/N cases.

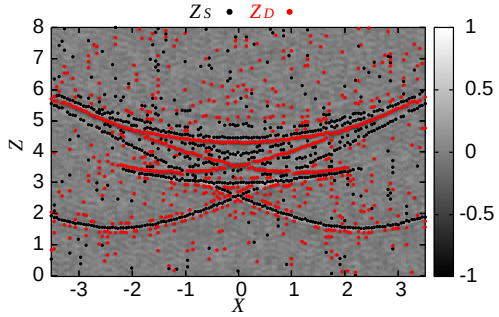

Fig. 7. Output of Wiener filter and extracted range points (X, Z_S) and (X, Z_D) for multiple ellipses at S/N=20 dB.

Here, the quantitative analysis is introduced by ϵ_i as,

$$\epsilon_i = \min_{\boldsymbol{p}_{\rm true}} \|\boldsymbol{p}_{\rm true} - \boldsymbol{p}_{\rm e}^i\|, \quad (i = 1, 2, ..., N_{\rm T}), \tag{6}$$

where $\boldsymbol{p}_{\rm true}$ and $\boldsymbol{p}_{\rm e}^i$ express the locations of the true and estimated target points not including the points obtained using RPM. $N_{\rm T}$ is the total number of $\boldsymbol{p}_{\rm e}^i$. Fig. 6 plots the number of estimated points for each value of ϵ_i in some S/N cases. It verifies that the proposed method significantly increases the number of target points with accuracy around 0.02λ, simultaneously enhancing the imaging range. The mean value of ϵ_i is 0.83λ for the conventional method S/N $= 20$ dB, and $2.9 \times 10^{-2}\lambda$, 4.9×10^{-2} and $6.2 \times 10^{-2}\lambda$ for the proposed method, at S/N $= 30$, 20 and 15 dB, respectively.

For the relevance of the proposed method, another target case, where three ellipses targets are assumed, is investigated. Figs. 8 and 9 show the estimated images produced by the conventional and proposed method, respectively, where the mean S/N is around 20 dB. As seen in these figures, the superiority of the proposed method is also clearly verified, in terms of stability to the random noises or interferences, and the side of the ellipse is accurately reproduced in such noisy and interfered situations.

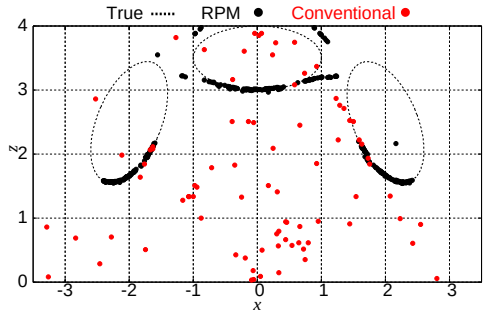

Fig. 8. Estimated image with RPM and the conventional method at S/N=20 dB for multiple ellipse objects.

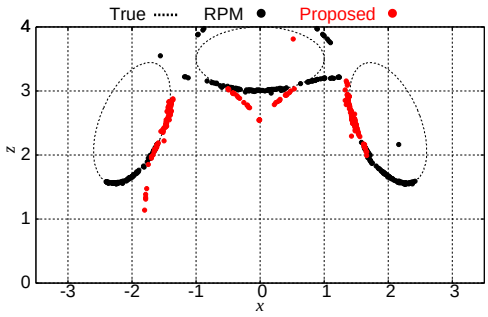

Fig. 9. Estimated image with RPM and the proposed method at S/N=20 dB for multiple ellipse objects.

6. CONCLUSION

This paper proposed the robust shadow region imaging algorithm, advancing the RPM principle to the doubly scattered signals. Our proposed method discarded the processing of derivative operation, which is sensitive to the small range fluctuations, and focused on the global distribution of the doubly scattered range points. Then, the numerical examples exemplify that the proposed method hold accuracy at the order of 1/100 λ, even for richly interfered situations and noisy situations, which significantly contributes the actual radar applications such as robotic or security sensors.

7. REFERENCES

[1] D. L. Mensa *et al.*, *IEEE Trans. Nuclear Science.*, vol. 27, no. 2, pp. 989–998, Apr, 1980.

[2] D. Liu, J. Krolik, and L. Carin, *IEEE Trans. Geosci. Remote Sens.*, vol.45, no.4, pp. 934–944, Apr, 2007.

[3] A. Massa *et al*, *IEEE Trans. Antenna Propagat.*, vol. 53, no. 10, pp. 3118–3127, Oct, 2005.

[4] S. Kidera, T. Sakamoto and T. Sato, *IEEE Trans. Geosci. Remote Sens.*, vol. 48, no. 4, pp. 1993-2004, Apr., 2010.

[5] S. Kidera, T. Sakamoto and T. Sato, *Proc. of PIERS 2009*, Vol. 5, No. 4, pp. 393–396, Aug, 2009.

[6] S. Kidera and T. Kirimoto, *IEEE Proc. of IGARSS 2011*, Jul., 2011.